Article

Electrolyte/Dye/TiO_2 Interfacial Structures of Dye-Sensitized Solar Cells Revealed by *In Situ* Neutron Reflectometry with Contrast Matching

Ke Deng, Jacqueline M. Cole,* Joshaniel F. K. Cooper, John R. P. Webster, Richard Haynes, Othman K. Al Bahri, Nina-Juliane Steinke, Shaoliang Guan, Liliana Stan, Xiaozhi Zhan, Tao Zhu, Daniel W. Nye, and Gavin B. G. Stenning

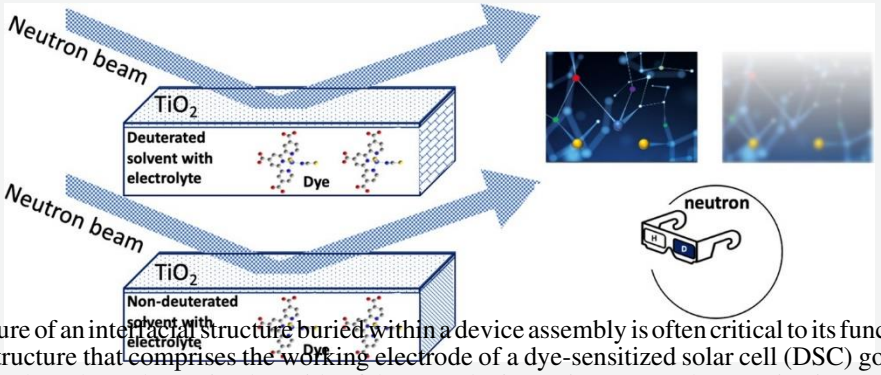

ABSTRACT: The nature of an interfacial structure buried within a device assembly is often critical to its function. For example, the dye/TiO_2 interfacial structure that comprises the working electrode of a dye-sensitized solar cell (DSC) governs its photovoltaic output. These structures have been determined outside of the DSC device, using *ex situ* characterization methods; yet, they really should be probed while held within a DSC since they are modulated by the device environment. Dye/TiO_2 structures will be particularly influenced by a layer of electrolyte ions that lies above the dye self-assembly. We show that electrolyte/dye/TiO_2 interfacial structures can be resolved using *in situ* neutron reflectometry with contrast matching. We find that electrolyte constituents ingress into the self-assembled monolayer of dye molecules that anchor onto TiO_2. Some dye/TiO_2 anchoring configurations are modulated by the formation of electrolyte/dye intermolecular interactions. These electrolyte-influencing structural changes will affect dye-regeneration and electron-injection DSC operational processes. This underpins the importance of this *in situ* structural determination of electrolyte/dye/TiO_2 interfaces within representative DSC device environments.

INTRODUCTION

Dye-sensitized solar cells (DSCs) are a photovoltaic technology whose transparency and flexibility affords them applications as solar-powered windows[1−3] or textiles for wearables.[4−7] Despite their potential, the interfacial structures within these devices, which govern their photovoltaic performance, are poorly understood at the molecular level.

A myriad of *ex situ* materials characterization methods has been employed to determine the interfacial structure of DSC working electrodes outside of the device, including imaging (atomic force microscopy,[8−11] scanning tunneling microscopy (STM)[12,13]), X-ray scattering (grazing-incidence X-ray scattering,[14] X-ray reflectometry (XRR)[10,15−18]), X-ray diffraction,[19−24] and optical,[25] vibrational (infrared (IR) and Raman),[26−28] X-ray absorption,[29−31] and photoelectron spectroscopy.[32,33] These studies have managed to quantify the essence of dye/TiO_2 interfacial structures that represent an exposed DSC working electrode. However, none of them have been able to directly probe this dye/TiO_2 interfacial structure while it is held within its DSC device assembly. This is because the dye/TiO_2 interface is buried within a DSC, so it is tricky to access nondestructively.

We need an *in situ* material characterization method to provide such quantification, since it is known that dye/TiO_2 structures will be modulated once contained within a DSC; such perturbations will affect their photovoltaic output.

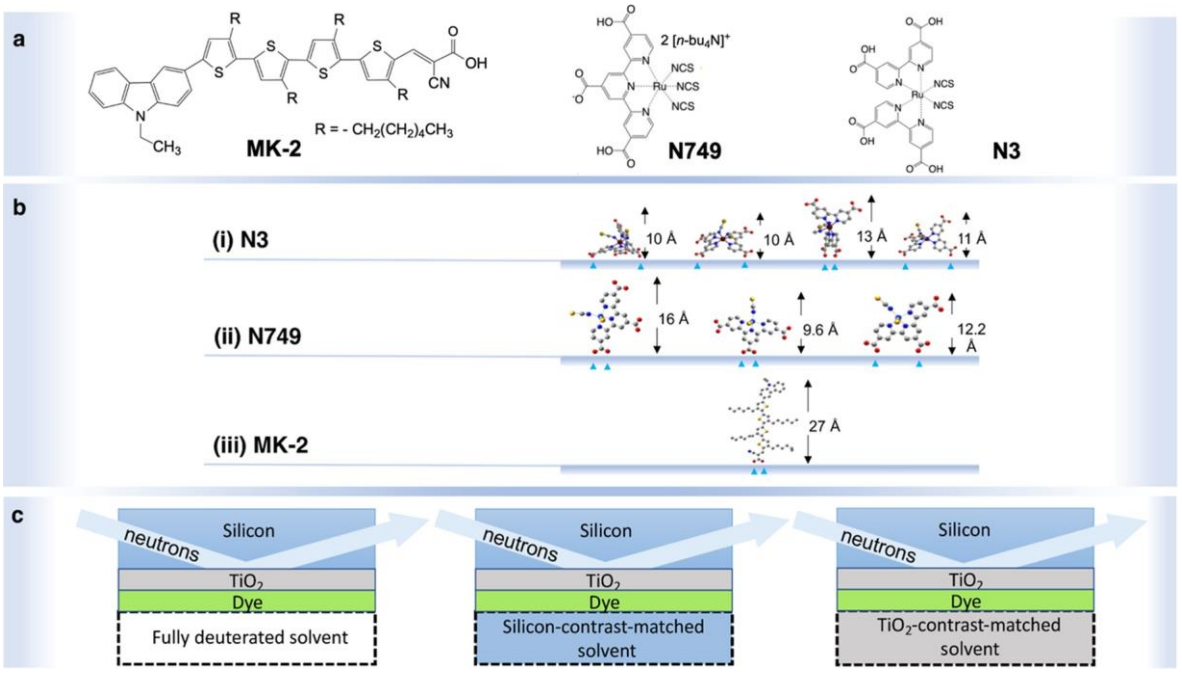

Figure 1. (a) Chemical schematic diagrams of the three dyes, MK-2, N749, and N3, used in this case study. (b) Dye/TiO_2 anchoring options for N3, N749 and MK-2. (c) Dye/TiO_2 device interface sandwiched between a silicon layer (to ensure good neutron transmission) and a solvent layer whose H/D ratio provides high contrast variation (left), contrast matching to the silicon layer (middle), or contrast matching to the TiO_2 layer (right).

Furthermore, their structure and function will be particularly influenced by a layer of electrolyte ions that lies above the dye self-assembly. Discerning the role of this electrolyte adds a chemical complexity to the problem while turning a single-interface problem into a binary electrolyte/dye/TiO_2 interfacial structure challenge.

We now solve this challenge using *in situ* neutron reflectometry with contrast matching. Neutrons can penetrate deep into devices, nondestructively, owing to their lack of charge. Neutrons are atomic probes that can decipher the nanoscopic structure of thin films buried within macroscopic devices, once aligned incident to a thin-film sample in a reflectometry geometry. Moreover, neutrons can target a particular part of a device, for example, a specific layer within a multilayered device where its material constituents are distinct from any other layer. Such targeting is possible because neutrons can discriminate between atoms of different elements and their isotopes. As such, neutron-scattering experiments can be designed to highlight particular device layers of interest by a process called contrast matching. This effectively blends the neutron-scattering contributions from one device region into another, by tuning the neutron-scattering differences between isotopes of a given element within one device layer, such that the overall scattering contribution from that layer equals that of another. The resulting zero differential-scattering contribution between two device layers helps the structural features of layers in between the contrast-matched layers to be highlighted. It also simplifies what is often a critically ill conditioned problem, whereby it reduces the number of data-refinement parameters that are needed to model a multilayered structure to a manageable level, and it provides multiple refinement options between differently contrast-matched (or not) data sets of that structure.

McCree-Grey and co-workers previously applied *in situ* neutron reflectometry to a DSC device assembly, with success in modeling its dye/TiO_2 interface;[17,34] while this used contrast variation, no layer was contrast-matched. We now show that this matching makes a critical difference to our ability to resolve an electrolyte/dye/TiO_2 interfacial structure in a DSC device. Thereby, the structural role of the electrolyte can be ascertained, while the dye coverage of the TiO_2 surface and the dye-to-TiO_2 anchoring configurations in a DSC can be determined at an unprecedented level.

EXPERIMENTAL DESIGN

Three dyes (Figure 1a) were used as case studies to demonstrate our approach: two quintessential high-performance ruthenium-based DSC dyes, the industrial standard N3,[35] and the near-panchromatic dye, N749 (Black Dye),[36] as well as the organic thiophenylcarbazole-based dye, MK-2,[37,38] upon which the previous non-contrast-matched *in situ* neutron reflectometry study[17] was focused. MK-2 thus provides an internal benchmark for assuring consistency in our results and a comparative for our contrast-matching co-refinement strategy, as well as representing a study in its own right. Each dye was adsorbed (anchored) onto a TiO_2 surface by solution-based sensitization (see Methods). Their carboxylate ions enable this chemisorption. Where a dye contains multiple carboxylic acid groups, as per N3 and N749, it may adopt one or more distinct anchoring modes onto TiO_2 surfaces.[39,40] Figure 1b shows the options that are considered most likely for each dye, based on findings from electronic-structure calculations and *ex situ* characterization of dye/TiO_2 interfacial structures.[9,41] Figure 1b also presents the lateral heights of each anchoring mode, which tend to differ. Reflectometry data can determine the lateral height of a dye layer,[10,15−18] since the thin-film thickness is a typical refinable data parameter. Thus, reflectometry was herein used to distinguish which anchoring mode dominates a dye self-assembly for N3 and N749.

Once a dye/TiO_2 working electrode had been installed within its DSC device assembly (Figure 1c), the dye/air interface was replaced by a dye/liquid interface. Prior to electrolyte addition, this liquid comprises a pure solvent solution; thus, at this point, the dye layer

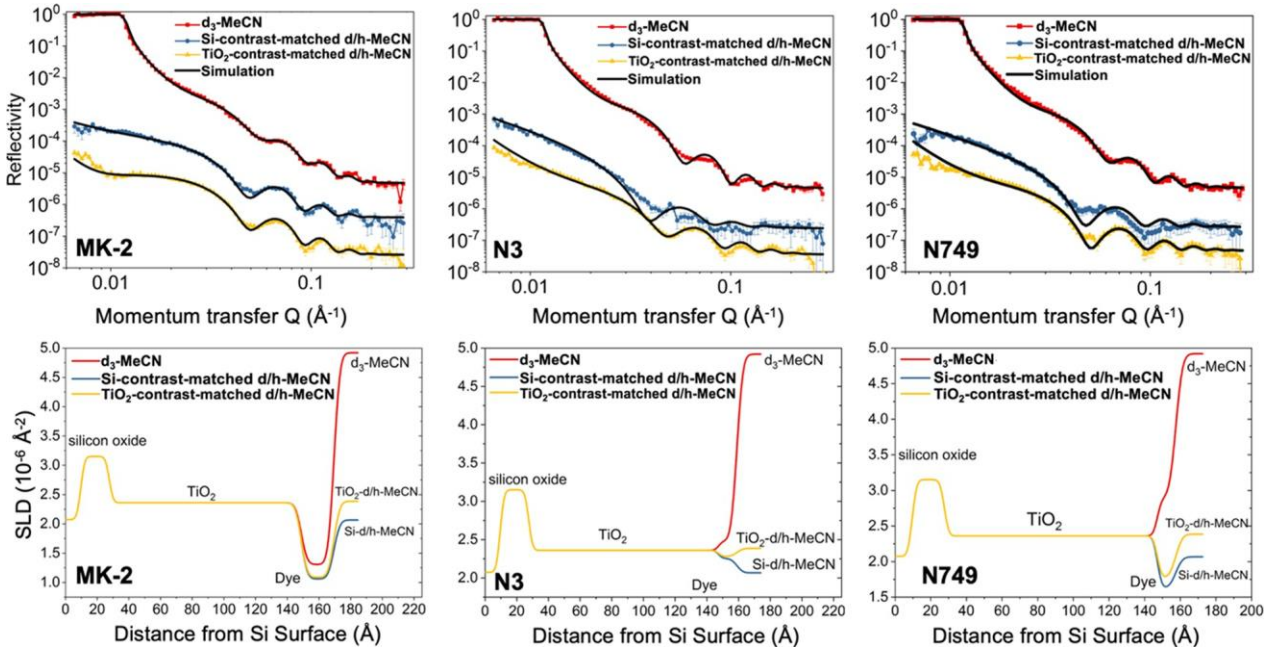

Figure 2. (Top) *Insitu* neutron reflectometry data of MK-2, N3, and N749 dye/TiO_2 interfaces and their fits to structural models that were determined by co-refining three sets of data per dye, which differ by the solvent residing above each dye layer having three different H/D ratios to produce two contrast-matching scenarios (TiO_2-contrast-matched d_3-MeCN and Si-contrast-matched d_3-MeCN/MeCN) and a fully deuterated d_3-MeCN environment that affords high contrast variation; (bottom) variation in neutron-scattering length density (SLD) for each dye/TiO_2 interface as a function of the position in the device assembly relative to the distance from the silicon surface; see also Figure 1c. It is worth noting that the fitting of the first trough in the reflectivity of the Si-contrast-matched data is compromised. This is because there is a tradeoff between the cost of background subtraction *versus* bringing the benefits of more apparent fringe features at higher Q (*cf.* the Sections S3 and S4, Supporting Information (SI)).

Table 1. Co-refined Structural Parameters of the Dye Layers (or the Top Layer Where Specified) for Two Contrast-Matching Scenarios (d_3-MeCN and Si-Contrast-Matched d_3-MeCN/MeCN) in the Presence of LiI or LiI/I_2 under Consideration of the Solvent Ingression in the Dye Layer as well as the Top Layer Where Specified[a]

		dye layer (or top layer where specified)				
dye	solution	thickness (Å)	fitting error for thickness (Å)	ρ_{dye} (10^{-4} unit/Å^3) or ρ_{top} (unit(I_2)/Å^3)	fitting error for ρ (10^{-5} unit/Å^3)	dye coverage φ_{dye} or electrolyte coverage φ_e (%)
MK-2	MeCN	20.6	−0.7, 0.8	5.84	−3.1, 3.5	91.4
	MeCN + LiI	20.6	−0.6, 0.8	5.86	−3.5, 2.6	87.8
	MeCN + LiI + I_2	20.8	−1.0, 0.9	5.97	−5.1, 6.5	62.7
	(top layer)	30.3	−1.0, 1.5	0.01025	−8.0, 6.9	11.8
N3	MeCN	11.5	−0.5, 0.5	9.95	−5.8, 7.3	92.1
	MeCN + LiI	11.6	−0.4, 0.5	9.75	−5.4, 8.2	78.8
	MeCN + LiI + I_2	13.3	−0.3, 0.3	9.90	−2.3, 2.1	99.7
	(top layer)	22.2	−0.4, 0.4	0.01054	−5.4, 8.2	4.5
N749	MeCN	10.3	−0.5, 0.3	7.63	−6.1, 5.5	55.7
	MeCN + LiI	10.9	−0.6, 0.8	7.74	−7.7, 8.0	36.3
	MeCN + LiI + I_2	12.5	−0.7, 0.7	12.81	−8.2, 3.6	99.9
	(top layer)	35.4	−1.2, 1.4	0.01066	−7.6, 4.1	5.5

[a]The "unit" density in the table is defined as the density per dye molecule or iodine. The neutron-scattering length density (SLD) of each dye layer can be derived by multiplying the fitted density of each dye layer with the total neutron-scattering length of one dye molecule.

may contain only dye and some solvent where it may ingress from the bounding liquid layer, whereby

$$SLD_{obs} = SLD_{dye}\varphi_{dye} + SLD_{svt}(1 - \varphi_{dye}) \quad (1)$$

where φ_{dye} is the fraction of the TiO_2 surface that is covered by the dye, which was also determined from reflectometry data using another refineable data parameter, the observed scattering length density (SLD_{obs}); the SLD values for the dye and solvent, SLD_{dye} and SLD_{svt}, respectively, were calculated directly from reference tables[42] according to their elemental constituents and isotopic composition.

The electrolyte was then added to the solvent solution. An I^-/I_3^- redox couple was selected for this purpose since it is by far the most commonly employed electrolyte in a DSC. These studies on how I^-/I_3^- would structurally influence the dye layer, and hence, the SLD was a matter for empirical modeling of these reflectometry data parameters.

Overall, our experimental design was thereby optimized such that our bespoke DSC device reflectometry setup could resolve these refinable dye-layer and SLD structural parameters to reveal the (a) preferred dye-anchoring configurations, (b) fraction of TiO_2 surface area that is covered by the dye, and (c) structural influence of the LiI

Table 2. Dye-Layer Thicknesses for MK-2, N3, and N749 Determined by Neutron and X-ray Reflectometry in This Work and in Previous Work Carried Out on the Same Dyes at the Same Sensitization Concentration (0.3 mM) and Time (20 h) and with the Same Solvents

dye-layer thickness (Å)	N3	N749	MK-2
this work			
in situ NR (Table 1, INTER, triple co-refinement)	11.5 + 0.5/−0.5	10.3 + 0.3/−0.5	20.6 + 0.8/−0.8
ex situ XRR (Table S1 (2))	10.7 + 0.3/−0.3	11.2 + 0.3/−0.1	19.4 + 0.7/−0.4
ex situ NR/XRR co-refinement (Table S1 (1))	10.4 + 0.2/−0.5	10.5 + 0.3/−0.2	19.5 + 1.0/−1.3
other work[17,18,34]			
in situ NR	11.8 ± 1.2		23.6 ± 1.9
ex situ XRR	10.2 ± 0.3		23.2 ± 0.2

electrolyte precursor and its fully-formed I^-/I_3^- redox couple on the dye self-assembly while held within its DSC device assembly.

The previous *in situ* neutron reflectometry study by Cole and co-workers[17] made it clear that the resolution of the dye-layer and SLD parameters needed to be improved, with their experimental errors reduced. These issues are especially acute if we want to resolve the structure of the extra interface that involves the electrolyte. We therefore adopted a twofold contrast-matching strategy that interrogates interfacial structures of DSC devices before and after electrolyte addition.

Determination of Solvent/Dye/TiO_2 Interfacial Structures. The first strategy exploits a triple co-refinement option to establish accurate dye-layer and SLD values for the baseline solvent/dye/TiO_2 interface prior to electrolyte addition.

Thereby, an acetonitrile (MeCN) solution was partially deuterated to provide the H/D isotopic variation needed for contrast matching this solvent layer to the silicon layer (d_3-MeCN/MeCN (20.8:79.2)) and subsequently to the TiO_2 layer (d_3-MeCN/MeCN (29.7:70.3)). These ratios afforded a "match point" whereby the positive and negative neutron-scattering contributions from deuterium and hydrogen, respectively, were tuned such that the SLD of the liquid (solvent) layer became equivalent to that of the silicon or TiO_2 layer. This produced two types of contrast-matched *in situ* neutron reflectometry data sets on solvent/dye/TiO_2 interfaces for each dye, while samples containing a fully deuterated d_3-MeCN solvent were also probed by *in situ* neutron reflectometry to offer analogous data sets with high contrast variation. Overall, this afforded three independent *in situ* neutron reflectometry data sets that were applied to a triple co-refinement to produce fits to structural models of solvent/dye/TiO_2 interfaces for each dye.

The results of this triple co-refinement of reflectometry data are shown in Figure 2 and Table 1. The dye-layer thickness of each solvent/dye/TiO_2 interface is smaller than at least one of its lateral heights shown in Figure 1, indicating that each dye forms a self-assembled monolayer, although it is not absolutely confirmed for N3 and N749 as their dye-layer thicknesses are slightly greater than the lateral heights of some of their anchoring options in Figure 1b. Moreover, the dye-layer thickness is closest to the lateral heights of the molecular configurations whose preferred anchoring mode when solvated in MeCN is anticipated for each dye from other work: bidentate bridging for N3,[18] Figure 1b(i)(4); anchoring *via* the central carboxylate ion for N749,[20] Figure 1b(ii)(2); and bidentate bridging carboxylate anchoring for MK-2, Figure 1b(iii)(1).[17] It is also worth noting that the various anchoring group options for N749 (*cf.* Figure 1b(ii)) are very close in energy when solvated in acetonitrile, with the bidentate bridging (Figure 1b(ii)(3)) and the monodentate end-on carboxylate anchoring modes (Figure 1b(ii)(1)) being only 0.05 eV apart; thus, there is potential for them to co-exist.[43] N3 and MK-2 dye self-assemblies cover over 90% of the TiO_2 surface, as deduced from SLD values (Table 1), while the 55.7:44.3 N749/acetonitrile ratio indicates that N749 dye self-assemblies are significantly less dense.

This model would suggest that N749 is affected markedly by solvent ingression. In theory, this could be the case since the N749 dye anion is bulky in three dimensions and yet it anchors through only one central carboxylate ion, furnishing it with spacious surroundings (Figure 1b(ii)). However, there is perhaps a more plausible explanation, remembering that N749 comprises two *tert*-butylammonium cations (TBA^+) per Ru-based anion. A TBA^+ cation could occupy a similar area on the TiO_2 surface compared to the Ru-based anion in N749, judging from related findings of TBA^+ influences on the dye self-assembly of N719.[18] Yet, TBA^+ cations in N749 are heavily disordered, even when contained within a crystal lattice such that they have not to be resolved by X-ray diffraction data.[20] While the motion of TBA^+ cations would be somewhat restricted within a dye self-assembled structure, this environment is less confined than a crystal lattice; thus, we could reasonably suppose that TBA^+ cations are also likely to be too dynamic to be resolved by reflectometry. Accordingly, *in situ* neutron reflectometry data models will only be able to observe the space that they occupy rather than the TBA^+ cations themselves. If TBA^+ cations lie in between N749 anions on TiO_2 surfaces, their "observation" will be erroneously attributed to the solvent since the calculation of φ_{dye} values uses the implicit assumption that the solvent is present wherever the dye anion (refined *via* SLD_{dye}) is absent. Therefore, the refined 55.7:44.3 N749/acetonitrile ratio obtained from our *in situ* neutron reflectometry data might be better re-categorized as an N749 anion/(acetonitrile + TBA^+) ratio.

Our findings on these solvent/dye/TiO_2 interfaces were compared with those from complementary *ex situ* X-ray reflectometry (XRR), as well as a concerted *ex situ* X-ray and neutron reflectometry co-refinement of data that we collected on the air/dye/TiO_2 interface (Tables 2 and S1). Our dye-layer thicknesses from *in situ* experiments are all larger (by up to 1.2 Å) than those obtained from complementary *ex situ* findings, with one exception (Table 2, *ex situ* XRR, N749). While these *ex situ* XRR and neutron reflectometry data display similar errors (Table 2), we expect the *ex situ* XRR data to be more reliable, since their Q-range is 4 times larger than that of neutron reflectometry and extends 2 more orders of magnitude in reflectivity (Figures S1–S3). Meanwhile, the errors of our triple co-refinement of *in situ* neutron reflectometry data are less than half of those achieved in the previous (not contrast-matched) *in situ* neutron reflectometry work (Table 2). Our MK-2 dye-layer thicknesses from *in situ* neutron reflectometry are also markedly more consistent with our *ex situ* results than with the previous *in situ* neutron reflectometry work. Our contrast-matching strategy has thus enabled a triple co-refinement of data on the solvent/dye/TiO_2 interface, which has an assured baseline accuracy for our *in situ* neutron reflectometry study.

Determination of Electrolyte/Dye/TiO_2 Interfacial Structures. We then sought to discern the electrolyte/dye/TiO_2 interfacial structure using the second contrast-matching strategy. Thereby, the I^-/I_3^- electrolyte redox couple was formed *in situ via* a two-stage process: (i) the electrolyte precursor, LiI, was injected into the solvent medium to generate I^- ions and (ii) I_2 was then added such that it reacts with I^- ions to form the fully functional electrolyte. *In situ* neutron reflectometry data were acquired (i) after LiI had been added and (ii) after I^-/I_3^- had formed to determine the influence of the electrolyte precursor and the fully formed I^-/I_3^- electrolyte. Data sets

for each two-stage process, for each dye, were collected in two solvent environments: fully deuterated MeCN and the silicon-matched 20.8:79.2 D/H ratio. This enabled a co-refinement of the reflectometry data shown in Figure 3.

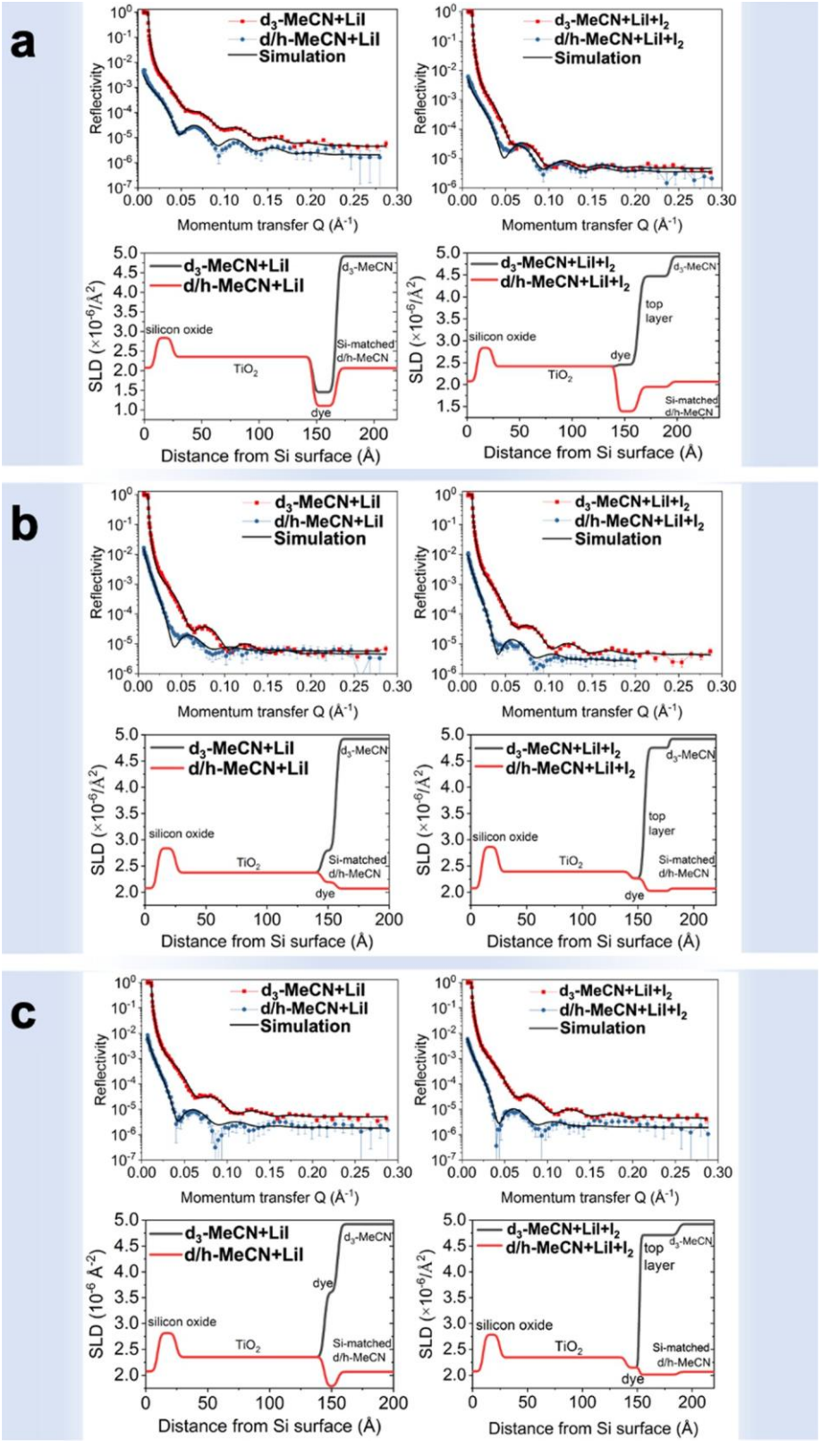

Figure 3. *In situ* neutron reflectometry data of (a) MK-2, (b) N3, and (c) N749 dye/TiO_2 interfaces and their fits to structural models that were determined by co-refining two sets of data per dye, which differ by the solvent residing above each dye layer having two different H/D ratios to produce a solvent layer that is contrast-matched to the silicon layer and a fully deuterated d_3-MeCN environment that affords high contrast variation; fits to the data shown on the left can be seen to improve once the "top layer" has been incorporated into the fit, as shown on the right. Plots underneath each reflectometry profile show the variation in neutron-scattering length density (SLD) for each electrolyte/dye/TiO_2 interface as a function of the position in the device assembly relative to the distance from the silicon surface; see also Figure 1c.

Electrolyte Ingression into the Dye Layers. Table 1 shows the results which reveal that N3 and N749 are substantially affected by the addition of I_2. While the change in dye-layer thickness is negligible upon the addition of the electrolyte precursor (LiI), there is a marked increase in the dye-layer thickness upon the formation of the fully functional electrolyte (Δ = 1.8 Å (N3); 1.6 Å (N749)); this contrasts starkly with the case of MK-2 (Δ = 0.2 Å). Indeed, the dye-layer thickness for MK-2 is practically identical for all three solutions containing MeCN, MeCN + LiI, or MeCN + LiI + I_2; this accords with the previous *in situ* neutron reflectometry study on MK-2.

Table 1 shows that φ_{dye} values for all three dyes decrease by a modest amount upon the addition of LiI, but a much larger change is observed when I_2 is added. φ_{dye} for MK-2 decreases upon I_2 addition by a larger margin than that observed for LiI addition. These changes in φ_{dye} for MK-2 track the expected trend for simple solvent dilution as LiI and I_2 electrolyte constituents are successively added. In contrast, φ_{dye} values for N3 and N749 are not reported in Table 1 since they refine to unrealistic values: 99.7 and 99.9%, respectively. These values actually signify that I_2 has ingressed into this layer, since the calculation of φ_{dye} assumed that the dye layer comprises exclusively the dye and solvent. Yet, these φ_{dye} values show otherwise; indeed, I_2 had just been added to the solvent to become a solute at this point. The SLD for I_2 (1.24×10^{-6} Å^{-2}) is substantially lower than the SLD for d_3-MeCN (4.90×10^{-6} Å^{-2}). Thus, the addition of I_2 with its subsequent ingression into a dye layer of N3 or N749 would artificially deplete its solvent contribution, owing to the influence of I_2 *via* its smaller SLD value, thereby artificially raising φ_{dye} (to >99%). Furthermore, we can be confident of the results since the use of contrast-matched and non-contrast-matched data makes the co-refinement particularly sensitive to the solvent medium with regards to the refinable SLD_{dye} parameter that is used to calculate φ_{dye}; this sensitivity occurs because the SLD for the dye and d_3-MeCN differ considerably, while the SLD_{dye} differs little with the Si-matched D/H MeCN dye solution data (Figure 3).

This I_2 ingression could explain the significant increase in the dye-layer thickness for N3 and N749 upon I_2 addition, especially given the dye-layer thickness of MK-2 remains constant under such conditions.[17] Within this scope, I_2 ingression may be associated with the NCS ligands on N3 and N749 forming [NCS]···I and [NCS]···I_2 interactions.[44] Indeed, their presence has been predicted for N3 by molecular-dynamics simulations, as well as infrared spectroscopy, which revealed a pronounced peak shift in the SCN vibrational mode of N3 once iodine had been added to a N3/TiO_2 DSC working electrode;[45] their associated structural models further indicate that these interactions manifest within [dye:I] and [dye:I_2] stable intermediates that form a key part of the redox process for N3. It is thought that these intermediates will dissociate upon reaction with I^- or I_2^- ions to form I_2^- or I_3^- ions. However, the stability of the [dye:I] and [dye:I_2] intermediates seems to allow us to detect these interactions *via* our *in situ* neutron reflectometry data through the manifestation of this I_2 ingression. The simulations display these [NCS]···I and [NCS]···I_2 interactions 3.12 and 2.83 Å apart, respectively. They will transfer electronic charge from the [NCS] to $[I_n]^-$ (n = 1 or 2), thereby acting as a process to deplete the electron density in the carboxylate dye/TiO_2 anchor and thus stand to increase the dye-layer thickness. Furthermore, each dye would presumably be subjected to steric effects, owing to this I_2 ingression and the corresponding [NCS]···I and [NCS]···I_2 interactions. These electronic and steric effects on the dye could readily disrupt the dye/TiO_2 binding. Indeed, the increase in dye-layer thickness for N3 upon I_2 addition, from 11.6 to 13.3 Å, is symptomatic of a considerable reorientation of the dye molecule such that it may well result in a change of dye/TiO_2 anchoring mode. Judging from the lateral heights in Figure 1b(i), it could involve a change from bidentate bridging *via* two carboxylate groups on different bipyridylcarboxylato (bpycoo) ligands (Figure 1b(i)(4)) to bidentate bridging *via* two carboxylate groups on the same bpycoo ligand (Figure 1b(i)(3)), or it could evolve to some form of monodentate carboxylate anchoring option from a mixture of bidentate bridging and monodentate binding modes realized by DFT studies.[24,46] The increase in dye-layer thickness for N749, from 10.9 to 12.5 Å upon I_2 addition, suggests that the molecular orientation of this dye likewise reorients considerably from an anchoring mode akin to that shown in Figure 1b(ii)(2) toward the configuration shown in Figure 1b(ii)(3); however, the tilting of the dye toward the TiO_2 is perhaps not quite sufficient to impart more than one carboxylate anchoring group onto the TiO_2 surface: *cf.* the thickness observed is 0.3 Å larger than that of the lateral height displayed in Figure 1b(ii)(3).

The aforementioned molecular-dynamics simulations[45] also predict that acetonitrile solvent will passivate the TiO_2 layer such that I^- ions cannot actually reach the TiO_2 surface upon I_2 ingression; the simulations further show that the closest approach of the I^- ions to the TiO_2 surface is *ca.* 5 Å while they mostly congregate at *ca.* 10 Å or around 13.0–15.5 Å from TiO_2 with a small, but narrow, distribution residing at *ca.* 6.5 Å. The N3 and N749 dye molecular reconfigurations associated with I_2 ingression, which are suggested above, would expose their NCS ligands more to I^- ions and I_2 (*cf.* Figure 1b), and the NCS ligand closest to the TiO_2 surface would reside at a lateral height of about a half of the total dye-layer thickness (*cf.* Figure 1b). The I^- ions of the corresponding [NCS]···I interactions would thus map well to the simulated small, but narrow, distribution of I^- ions centered at *ca.* 6.5 Å. Meanwhile, the pyridyl-containing ligands in N3 and N749 exhibit an open geometry toward the top of the lateral height of each dye, judging from Figure 1, thereby affording cavities at lateral heights that would correspond well to the simulated 10 and 13.0–15.5 Å distributions where the other I^- ions could presumably ingress. The molecular-dynamics simulations also showed that I^- ions exhibit a similar but far broader and less defined radial distribution function to that of I^- ions. Thus, I^- ions and I_2 molecules will presumably track a similar trend of ingression into the dye layer.

Layer of Iodo Species Atop the Dye Self-Assembly. The molecular-dynamics simulations for N3 also predict that a broader distribution of I^- ions extends up to *ca.* 22.0 Å from the TiO_2 surface, whereby a sharp drop in I^- concentration is observed.[45] This implies that there is a distinct layer atop the dye self-assembly, which contains electrolyte ions. Indeed, our *in situ* neutron reflectometry data on all three dyes that had been acquired after I_2 injection could not be refined adequately using the three-layer model (*cf.* Methods), which we have always adopted previously in our analysis of X-ray and neutron reflectometry data.[16−18] In contrast to these previous studies, our contrast-matching strategy employed herein allowed the resolution of an additional layer of material in the DSC device assembly, exclusively for the data acquired after I_2 had been added. This extra layer was modeled with a range of material options, but it was eventually found to wholly represent an electrolyte contribution. This electrolyte layer carried the following SLD model

$$SLD_{obs\_toplayer} = SLD_{electrolyte}\varphi_{electrolyte} + SLD_{svt}(1 - \varphi_{electrolyte})$$

where "electrolyte" refers to the constituents of the electrolyte precursor and the fully formed I^-/I_3^- redox couple. In principle, this will comprise I^- and I^- ions as well as its I^- constituent and some I^- that befits the low-energy configurations of N3 on (101) TiO_2

residual Li^+ ions. However, supporting *ex situ* X-ray and neutron reflectometry data acquired on these same DSC dye assemblies once they had been dried out, *i.e.*, once the solvent had been removed by evaporation, suggest that iodo species constitute the electrolyte contribution almost exclusively (see Section S2, Supporting Information).

Table 1 shows the parameter characteristics of this top layer of iodo species in acetonitrile solvent. These were obtained from co- refinement of our *in situ* neutron reflectometry data on samples containing solvents that exhibit high contrast variation, *i.e.*, d_3-MeCN and Si-matched D/H MeCN solvent media. The electrolyte coverage, φ_e, for this top layer (11.8% for MK-2, 4.5% for N3, 5.5% for N749) shows that the iodo species are sparsely populated within acetonitrile solvent, on top of each dye self-assembly. Moreover, the φ_e values for N3 and N749 are more than half that of MK-2; this stands to reason since a fixed quantity of electrolyte constituents was added to each

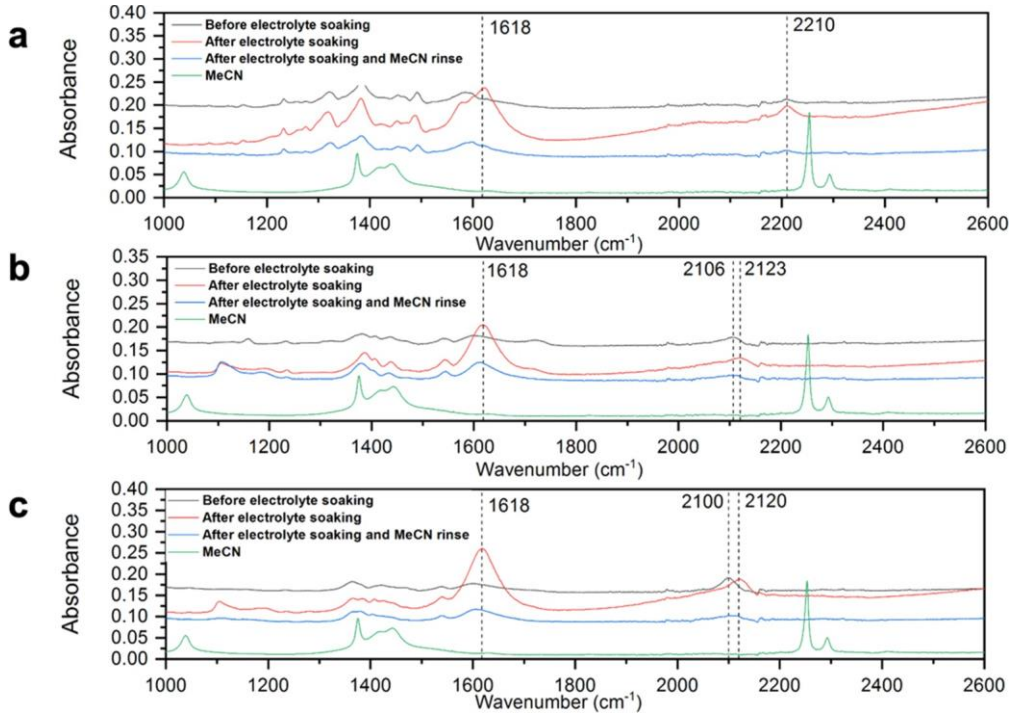

Figure 4. *Ex situ* Fourier transform infrared data of (a) MK-2, (b) N3, and (c) N749 dye/TiO_2 interfaces on indium tin oxide (ITO)-glass substrates, before and after the electrolyte has been added.

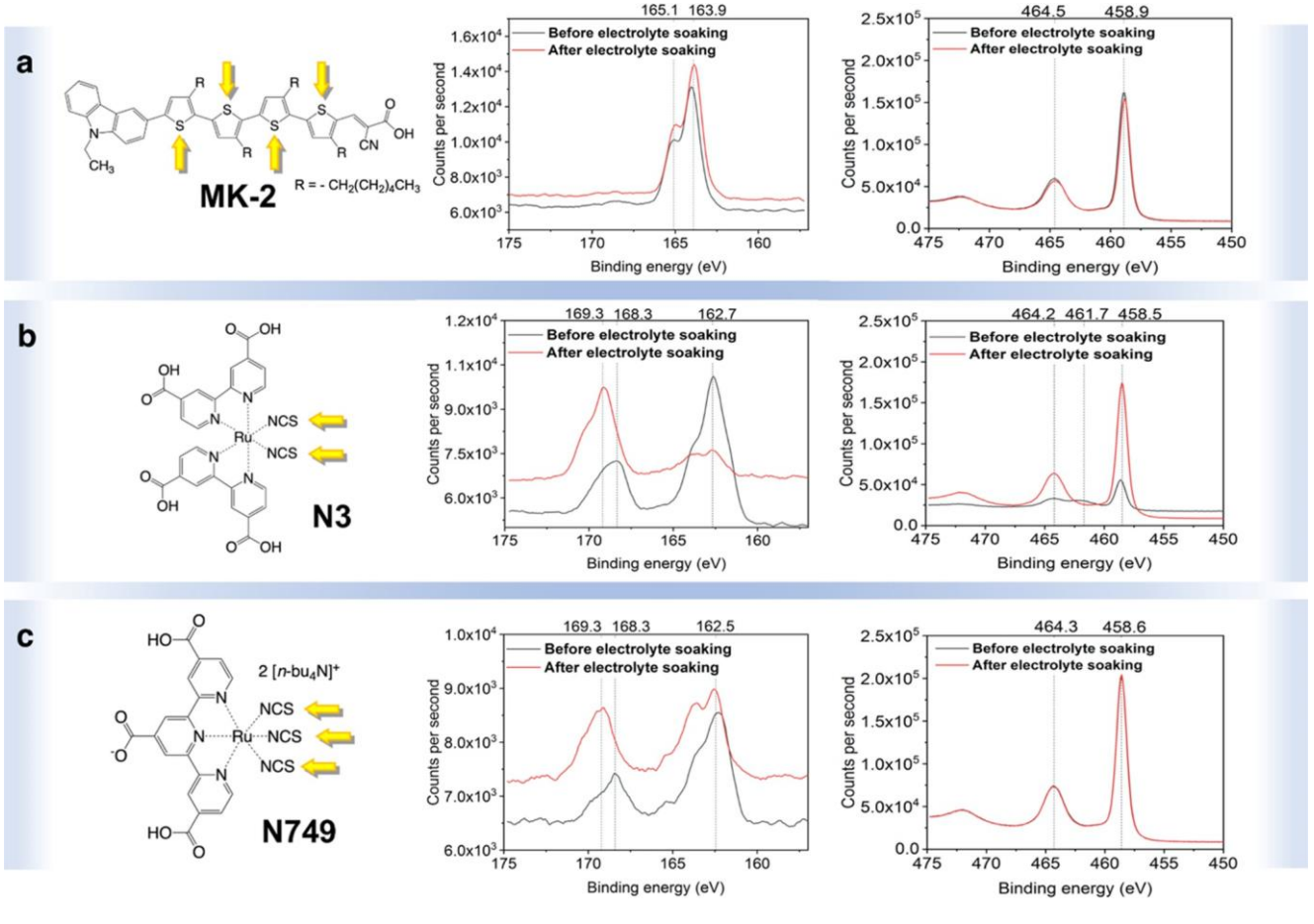

Figure 5. *Ex situ* X-ray photoelectron spectroscopy data of (a) MK-2, (b) N3, and (c) N749 dye/TiO_2 interfaces on ITO-glass substrates, before and after the electrolyte has been added. Yellow arrows highlight the sulfurs in each dye molecule (left) that influence the XPS 2p S spectra (middle); corresponding XPS 2p Ti spectra are shown on the right.

DSC device assembly and, unlike MK-2, iodo species ingress into the N3 and N749 dye layers, leaving less in the top layer.

The refined thickness parameter of each top layer shows that these solvated iodo species lie above the dye layer by 30.3 Å (MK-2), 22.2 Å (N3), and 35.4 Å (N749). The different thicknesses for N3 and MK-2 may indicate that the lateral height of this top layer is affected by the solvent concentration of the iodo species; after all, I_2 ingression into the dye layer was observed for N3 but not for MK-2, so the top layer of MK-2 will presumably contain substantially more iodo species than those of N3. Indeed, the iodo species coverage, φ_e, of the top layer for MK-2 is about double that of N3.

One would instinctively think that the iodo species in the top layer for N749 would manifest similarly to that of N3. Indeed, the results above show that I_2 ingresses into the dye layer for N749 in a fashion similar to that of N3; also, the top layer for N3 and N749 evidences a similar coverage, φ_e. However, the thickness of the top layer for N749 refines to nearly double that of N3, even though these two dye anions are chemically similar. The same dye concentrations were used for each DSC device assembly, and the amount of solvated iodo species added to the device environment was the same. Thus, the most logical explanation for this difference would seem to involve some effect that is not part of the model. N749 contains two TBA^+ cations per Ru-based anion, and we saw earlier that there might be a latent manifestation of TBA^+ cations in the dye layer when N749 is surrounded purely by acetonitrile. Once I_2 has been injected into the DSC device assembly, N749 will partially oxidize, owing to the formation of stable [NCS]···I or [NCS]···I_2 interactions; this oxidation stands to displace at least some of the TBA^+ cations in the dye self-assembly, and these TBA^+ cations will also be electrostatically attracted to the I^-/I_3^- ions that ingress into the dye layer and in the top layer just above.[3] Additionally, TBA^+ cations are unbound to the TiO_2 surface and so will be somewhat labile. Thus, they may be able to diffuse into the top layer; they may also be involved in ion exchange with Li^+ ions from the electrolyte constituent. The co-refinement of our neutron reflectometry data using the four-layer model for N749 actually affords the best figure of merit of all refinements herein. It would thus seem that our data do not see the TBA^+ cations; this is consistent with our observations (vide supra) that these ions are too dynamic to be modeled using our reflectometry data. They will nonetheless manifest as an occupied space that is erroneously attributed to the iodo species in the top layer. This could readily explain the much greater top layer thickness for N749 of 35.4 Å compared with that of N3.

Corroboratory Evidence from *Ex Situ* Fourier Transform Infrared (FTIR)-Attenuated Total Reflectance (ATR) and X-ray Photoelectron Spectroscopy (XPS) Experiments. The presence of these dye/electrolyte interactions, indicated by our *in situ* neutron reflectometry results, was corroborated by *ex situ* attenuated total reflectance-Fourier transform infrared (ATR-FTIR) and X-ray photoelectron spectroscopy (XPS) of dye/TiO_2 DSC working electrodes before and after a (dried out) soaking in an electrolyte solution.

Figure 4 displays the ATR-FTIR spectra of each dye. Both show that the addition of the electrolyte up-shifts the vibrational frequency of the C≡N stretch for the NCS ligands[47] in N3 and N749 from ~2100 to 2120 cm^{-1}, which corroborates the formation of [NCS]···I and [NCS]···I_2 interactions. MK-2 shows no such absorption in this range, being void of NCS groups, but it does exhibit a vibrational stretch due to its C≡N group[48] at 2210 cm^{-1}. All three dyes display asymmetric C=O stretches centered at 1618 cm^{-1}. Figure 4 also shows that rinsing the substrates with neat MeCN depletes all of the features associated with these vibrational modes, thereby supporting these dye and electrolyte assignments.

Figure 5 displays the S and Ti XPS spectra of all three dyes. The XPS S 2p spectra support the formation of [NCS]···I and [NCS]···I_2 dye/electrolyte interactions upon the addition of the I^-/I_3^- redox couple to N3- and N749-containing DSC device assemblies. Thereby, the XPS S 2p broad peak signatures centered at 168.3 eV for both dyes increase to 169.3 eV upon electrolyte addition. This shift in binding energies is characteristic of the partial oxidization of sulfur,[49] as would feature in the [NCS]···I and [NCS]···I_2 interactions since they will promote charge transfer from the isothiocyanate ion to the iodo species. N3 loses nearly all of its nonoxidized XPS S 2p peak signature, centered at 162.7 eV, to this oxidized form, upon electrolyte addition, suggesting that both of its NCS ligands form [NCS]···I_n (n = 1 or 2) interactions. In contrast, XPS S 2p spectra of N749 partially show the same trend as those of N3; yet, the majority of isothiocyanate ligands in N749 do not interact with the electrolyte, as evidenced by its nonoxidized XPS S 2p peak signature, centered at 162.5 eV, whose integral is larger than that of its oxidized structural signature, after electrolyte addition. The analogous XPS S 2p spectra of MK-2 evidence no such peak; rather, they display nicely resolved, classic XPS S $2p_{1/2}$ and $2p_{3/2}$ peak doublets,[49] centered at 163.9 and 165.1 eV, indicating that its thiophenyl S atoms in MK-2 are entirely stable to oxidation, as expected.

With one stark exception, XPS Ti spectra show the classic $2p_{1/2}$ and $2p_{3/2}$ peak doublet signature for all dyes before and after electrolyte addition; their binding energies cover a narrow range, whereby the large and small peaks are centered at 458.5–458.9 and 464.2–464.5 eV, respectively; their peak intensities are similar for the three dyes. All of these factors indicate that the chemical environment, by which the Ti interacts with carboxylate ions, is essentially the same for each dye in the presence or absence of an electrolyte, with one stark exception. This exception concerns N3 on TiO_2 prior to electrolyte addition. The intensities of both peaks are low, while its higher-energy peak is broad and carries a peak shoulder centered at 461.7 eV. This suggests that N3 anchors to TiO_2 in several different chemical environments prior to I_2 addition, as per the bidentate bridging anchoring configuration of N3-adsorbed TiO_2, which involves two distinct carboxylate groups (Figure 1b(i)). This is in agreement with a range of *ex situ* material characterization and electronic-structure calculations, including other reports of *ex situ* XPS Ti 2p spectra of N3 on TiO_2, which likewise reveal two weak peaks, with its higher-energy peak being particularly broad.[50,51] A pioneering *ex situ* STM/scanning tunneling spectroscopy (STS) experiment also showed that N3 could co-exist in at least five molecular configurations on an idealized (101) TiO_2 surface.[13] Our *in situ* neutron reflectometry results, combined with those of the *ex situ* XPS Ti 2p study, suggest that the anchoring mode of N3 on TiO_2 changes once it has been covered by the fully formed electrolyte such that the dye-reconfigures to a different orientation on the TiO_2 surface as indicated by (i) a change in dye layer thickness observed by the neutron reflectometry and (ii) a change in electronic states of titanium and sulfur atoms observed in the XPS results, in a fashion that affords a single type of anchoring as suggested by Figure 1b(i). This exhibits an essentially identical chemical environment to the anchoring modes of MK-2 and N749 within the vicinity of the TiO_2 surface. Given that N749 and MK-2 exhibit bidentate bridging anchoring *via* a single carboxylate group, it would thus seem that N3 changes to the same form of bidentate bridging carboxylate anchoring mode upon I_2 addition.

Influence of the Electrolyte on Interfacial Structures of DSC Device Environments. As discussed above, our *in situ* neutron reflectometry studies indicate that the nature of anchoring for N3 on TiO_2 within a DSC device assembly also changes upon I_2 addition, given the change in dye-layer thickness observed. The formation of stable [NCS]···I and [NCS]···I_2 interactions was deemed responsible for this disruption in dye/TiO_2 anchoring. Given this change in dye-layer thickness and the fact that our XPS S 2p and Ti 2p results both corroborate the formation of these interactions upon electrolyte addition, we conclude that the N3 anchoring group does indeed change within the DSC device assembly once exposed to the electrolyte. The extent of modulation in dye-layer thickness upon I_2 addition suggested that the dye may change from bidentate bridging *via* two carboxylate groups on different bpycoo ligands (Figure 1b(i)(4)) to either bidentate bridging *via* two carboxylate groups on the same bpycoo ligand (Figure 1b(i)(3)) or some form of a bidentate bridging mode *via* the same carboxylate group. The corroboratory evidence from XPS Ti 2p studies indicates that the most plausible option is that N3 changes to a bidentate bridging anchoring mode through one carboxylate group upon I_2 addition. It

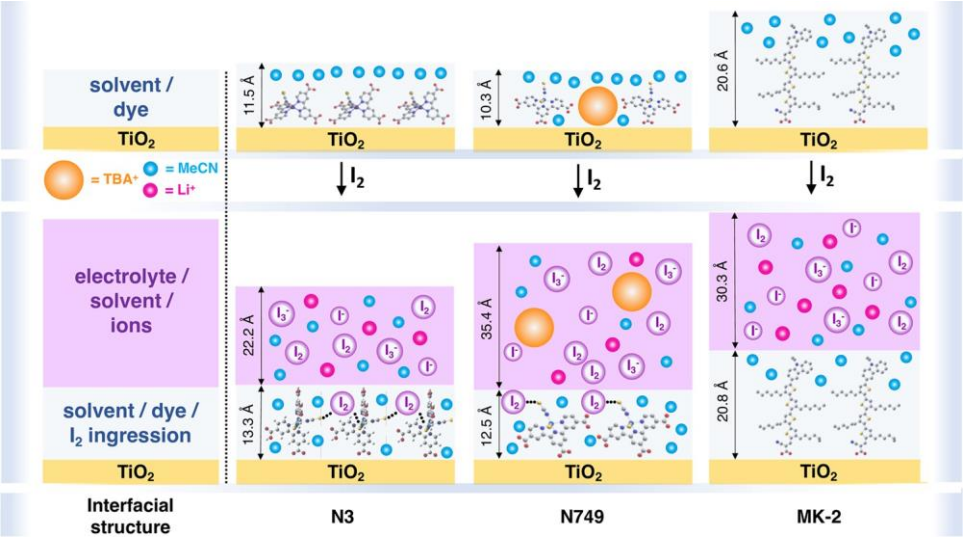

Figure 6. Ensemble model of the acetonitrile/dye/TiO_2 and electrolyte/dye/TiO_2 interfacial structures determined by this *in situ* neutron reflectometry study. The model accounts for all experimental findings except for the precise whereabouts of the Li^+ ions and the iodide ions within the dye layers. They have been added to the top layer in this illustration since they must be present somewhere within the device environment, even though the neutron-scattering signatures show no evidence for them. The presumption is that they will reside in the top layer together with the other solvated ions since there is no indication that they ingress into the dye layer.

would seem that this change in anchoring mode requires minimal energy, judging from electronic-structure calculations; for example, at least three bidentate bridging and monodentate anchoring options of N3 are deemed to lie close in energy when modeled in vacuo.[46]

The molecular-level mechanism behind this electrolyte influence presumably originates from the [NCS]···I and [NCS]···I_2 interactions competing with dye/TiO_2 adsorption since they both involve charge donation away from N3. For charge-balancing reasons, a different anchoring mode of N3 may thus become more electronically stable once an I^-/I_3^- electrolyte layer lies atop its dye self-assembly. This would explain the marked increase in the dye-layer thickness of N3 upon the addition of I_2 that we see in our *in situ* neutron reflectometry results (Table 1). Therein, N749 displayed a similar jump in its dye-layer thickness, but the nature of its anchoring group is considered to be different from that of N3 prior to I_2 addition. Thus, the two cases are not expected to be influenced in the same way; indeed, N749 displays only partial oxidation of the sulfur in its NCS ligands, while N3 evidences complete oxidation. Meanwhile, the molecular behavior of MK-2 is minimally impacted by its incorporation into a DSC device.

These reflectometry findings show how the electrolyte may influence the structural geometry of the dye and the dye/TiO_2 interface. They complement well recent studies that have investigated the dynamics of electron recombination and dye regeneration in DSCs, whose mechanisms appear to involve dye/electrolyte bonding interactions.[52−54]

Figure 6 summarizes the overarching acetonitrile/dye/TiO_2 and electrolyte/dye/TiO_2 interfacial structures determined by this *in situ* neutron reflectometry study.

METHODS

Preparation of Thin Films of Amorphous TiO_2. Atomically flat amorphous thin films of TiO_2 were prepared using atomic layer deposition (ALD) at the Center of Nanoscale Materials, Argonne National Laboratory. Amorphous TiO_2 films (thickness: 12 nm) with atomically flat surfaces were deposited on silicon wafer substrates using an Arradiance Gemstar ALD instrument. Tetrakisdimethylamido-titanium (TDMAT, 99.999%, Strem Chemicals) was reacted with H_2O. The TDMAT precursor was heated to 60 °C, while the H_2O was kept at room temperature. High-purity nitrogen gas (99.999%) was used as carrying and purging gases with flow rates of 40 and 100 sccm, respectively. The temperatures of the reactor chamber and the sample holder were maintained at 200 °C. During the exposure-mode ALD process, the evacuation valve was closed before introducing the precursor in the chamber and opened after a delay time. A cycle consisted of 0.7 s TDMAT pulse, 1.3 s delay, 23 s N_2 purge, 0.022 s H_2O pulse, 1 s delay, and 28 s N_2 purge. The TiO_2 deposition rate was about 0.38 Å/cycle. The 12 nm TiO_2 film thicknesses showed high uniformity across all samples, as confirmed by X-ray reflectometry.

Fabrication of Dye/TiO_2 Working Electrodes. The ALD-prepared thin films of TiO_2 on silicon wafer substrates were sensitized with each dye. This involved immersing the wafers into a 0.3 mM solution of each dye for 20 h; acetonitrile/*tert*-butanol/toluene (1:1:1, v/v) was used for MK-2 (95%, Sigma-Aldrich), while acetonitrile/*tert*-butanol (1:1, v/v) was used for N3 (95%, Sigma-Aldrich) and N749 (95%, Solaronix). All solvents (ACS reagent grade) were purchased from Sigma-Aldrich. Sensitized wafers were subsequently rinsed with neat acetonitrile (10 s) and dried under a flow of N_2 prior to the *in situ* and *ex situ* measurements.

Preparation of DSC Counter Electrodes. Fluorine-doped tin oxide (FTO) glass counter electrodes with platinum as the electron-transfer catalyst were prepared. This required drop-casting a 5 mM solution of chloroplatinic acid hydrate (99.995%, Sigma-Aldrich) in isopropanol (ACS reagent grade, Sigma-Aldrich) onto clean FTO glass slides (TEC 8, Sigma-Aldrich, 90 × 90 × 3.2 mm^3), which were subsequently heated for 15 min at 390 °C.

Preparation of Electrolyte Solutions. Solutions of 0.7 M lithium iodide (LiI) (99.9%, Sigma-Aldrich) and 0.05 M iodine (I_2; 99.99%, Sigma-Aldrich) were mixed in a solvent to form the active I^-/I_3^- redox electrolyte. In the neutron reflectometry studies, non-deuterated acetonitrile (MeCN) (ACS reagent grade, Sigma-Aldrich) and d_3-acetonitrile (99.8%, Sigma-Aldrich) were the solvents employed; their deuterated nature enables sufficient neutron-scattering contrast of the buried interface within each sample under investigation. Nondeuterated MeCN (ACS reagent grade, Sigma-Aldrich) provided the solvent media for the active I^-/I_3^- redox electrolytes in the FTIR and XPS studies.

Preparation and Sensitization of Nanoparticulate TiO_2. Neither XPS nor IR measurements mandated atomically flat, amorphous TiO_2 films. Moreover, XPS and IR signals would benefit from a sample that contains a much thicker (μm) TiO_2 film. XPS and IR results on the nanoporous TiO_2 can also complement our neutron reflectometry results on atomically flat DSCs to provide insights that

are comparable to fully operational DSCs. Therefore, nanocrystalline thin films of TiO_2 were prepared for these measurements. Thereby, thin films of nanocrystalline TiO_2 were fabricated by initially depositing one layer of nanoparticulate TiO_2 paste (Dyesol, DSL 18NR-T) onto a clean ITO-coated glass substrate (1 × 1 cm^2, Sigma-Aldrich) using the doctor-blade technique with tape to set boundaries and control the TiO_2 thickness to around 10 μm. Sintering this paste at 500 °C for 30 min yielded nanoporous films of TiO_2. These films were then submersed in a 0.5 mM solution of MK-2 (95%, Sigma-Aldrich) in MeCN/*tert*-butanol/toluene (1:1:1, v/v) or in 0.5 mM solutions of N3 (95%, Dyesol) or N749 (95%, Solaronix) in MeCN/*tert*-butanol (1:1, v/v) for 20 h; all solvents (ACS reagent grade) were purchased from Sigma-Aldrich. Thereafter, the substrates were rinsed with neat MeCN and dried under a flow of nitrogen gas. An active dye/TiO_2 working-electrode surface area of ∼1 cm^2 was created *via* the removal of excess TiO_2 from the periphery of the parent film.

Contrast-Matched *In Situ* Neutron Reflectometry on the INTER Instrument. *In situ* neutron reflectometry measurements were conducted using the high-intensity INTER reflectometer at the ISIS Neutron and Muon Source, U.K.[55] This instrument was equipped with a low-background ^{3}He gas detector, and beam profiles were collected at the sample angle θ = 0.5 and 2°. Measurements were conducted on thin films of amorphous TiO_2 sensitized with MK-2, N3, or N749. Data were reduced using the Mantid software.[56] Background subtractions were performed, as detailed in the Supporting Information (Sections S3 and S4). The *in situ* neutron reflectometry data were plotted as a function of the momentum transfer vector (Q) perpendicular to the TiO_2 surface according to $Q = 4\pi \sin\theta/\lambda$, where θ is the incident angle and λ is the wavelength of the neutrons. A schematic diagram of the sample measurement geometry is shown in the Supporting Information (Figure S9, Section S5), while the beam size and profile are shown in Figure S10.

The substrates are 3-in.-diameter n-type silicon (100) wafers (thickness: ≥5 mm), which ensures an uninterrupted beam transmission and avoids excessive attenuation of the neutron beam. The determination of the thickness of the SiO_2 substrate is described in the Supporting Information (Section S6). Deuterated acetonitrile (d_3-MeCN) was used to enhance the contrast between the dye and the electrolyte. Nominal values for the neutron SLD of each layer were used to construct initial structural models using a three-layer approach. For the substrates, values of 2.07×10^{-6}, 3.48×10^{-6}, and 2.39×10^{-6} $Å^{-2}$ were used for the silicon wafer, the native oxide layer, and the TiO_2 layer, respectively. The SLD of the subphase solvent d_3-MeCN was set to 4.92×10^{-6} $Å^{-2}$. All TiO_2 film thicknesses were refined to 12 nm (*cf.* Table S2, Section S7, Supporting Information).

Contrast matching represents an effective way of using the power of neutron reflection. Mixing CH_3CN with CD_3CN (d_3-MeCN) afforded acetonitrile with different H/D ratios, which eventually furnished solvent contrasts similar to those of silicon (d_3-MeCN/MeCN (20.8:79.2)) and TiO_2 (d_3-MeCN/MeCN (29.7:70.3)). Contrast matching silicon allows examining exclusively the dye···TiO_2 interface and the native oxide layer, while contrast matching TiO_2 allows examining exclusively the dye layer and the silicon substrate with the native oxide layer.

The reduced data were refined using GenX,[57] which employs a differential evolutional algorithm to perform robust optimization and avoid local minima. The three-layer model that we had previously used was no longer adequate once I_2 was added (*cf.* Figure S12, Section S7, Supporting Information). For example, the addition of I_2 leads to a substantial increase of the roughness of the MK-2···solvent interface, as seen from the drastic reduction of SLD variation steepness at the dye···solvent interface and the distortion of the SLD profile at the MK-2···TiO_2 interface (Figure S12a). This interpretation would also be consistent with the considerably high fitted MK-2···solvent interfacial roughness value (19.8 Å) shown in Table S2 for the three-layer model. Even though the three-layer fitting sample model assumes no extra layer on top of the dye, it has the limitation as the MK-2···solvent interfacial roughness value is almost comparable to the thickness of a dye layer, and the MK-2···solvent interfacial roughness could tentatively be explained by the formation of an iodo top layer. Once an extra iodo top layer is added to the fitting model, the resulting four-layer model of the neutron reflectometry data for MK-2 affords reasonable interfacial roughness values, especially considering the roughness of the dye···solvent interface (∼2 Å); *cf.* 19.8 Å for the model without this extra top layer. Thus, the new four-layer model detailed above is a better representation of the true model.

Ex Situ Neutron Reflectometry. *Ex situ* air−solid neutron reflectometry measurements were carried out using the single-frame (2.0 Å < λ < 7 Å) mode of a time-of-flight neutron reflectometer, *i.e.*, the multipurpose reflectometer (MR) at the China Spallation Neutron Source (CSNS).[58−60] Reflected neutron beam spectra were recorded on a two-dimensional (2D) position-sensitive ^{3}He area detector with an active area of 20 × 20 cm^2 and a spatial resolution of 2.2 mm. Incident neutron angles of 0.3, 0.6, or 1.2° were used to cover the Q-range required for these data. Direct beam measurements were collected under the same collimation conditions. Neutron reflectometry data were fitted using the default layer model in GenX. The neutron SLD profiles along the normal direction of the films were extracted. These neutron reflectometry experiments at CSNS used the same samples as those employed for the NR work on the INTER reflectometer at the ISIS Neutron and Muon Source, with two exceptions: the electrolyte constituents from the samples for the INTER experiments were all removed prior to the CSNS experiments by rinsing the dye-sensitized substrates with the same solvent that had been used in the INTER experiments. Further details about this procedure and its influence are provided in the Supporting Information (Section S1).

Ex Situ X-ray Reflectometry. X-ray reflectometry measurements were conducted using a Rigaku SmartLab reflectometer (9 kW rotating anode; Cu Kα X-ray source; λ = 1.541 Å) equipped with a Ge (220 × 2) monochromator. X-ray reflectivity data were collected in increments of 0.01° for a detector range of 0.1° < 2θ < 8°. Nominal values for the X-ray SLD of each layer were used to construct initial structural models based on a three-layer approach. For the substrates, SLD values of 20.1×10^{-6}, 18.9×10^{-6}, and 31.2×10^{-6} $Å^{-2}$ were used for the silicon wafer, the native oxide layer, and the TiO_2 layer, respectively. By fitting the X-ray reflectivity data, the thickness of the MK-2, N3, and N749 dye layers on 12 nm thick films of amorphous TiO_2 (*cf.* Table S2) were determined.

X-ray Photoelectron Spectroscopy. X-ray photoelectron spectroscopy measurements were performed on a Thermo Fisher Scientific NEXSA spectrometer under high vacuum ($P \sim 10^{-8}$ mbar) with thin-film samples of nanoparticulate TiO_2 on silicon substrates sensitized with each DSC dye, prepared as detailed. Samples were analyzed using a microfocused monochromatic Al X-ray source (72 W) with an oval spot size of approximately 200 × 100 $μm^2$. Data were recorded at pass energies of 200 eV for survey scans and 50 eV for high-resolution scans in increments of 1 and 0.1 eV, respectively. Charge neutralization of the sample was achieved using a combination of both low-energy electrons and argon ions.

Attenuated Total Reflection (ATR)-Fourier Transform Infrared (FTIR) Spectroscopy. ATR-FTIR measurements were performed on thin films of nanoparticulate TiO_2 on silicon substrates sensitized with each DSC dye using a Nicolet iS 10 FTIR spectrometer. The substrates were clamped by a Smart iTX tip on top of a highly refracting crystal through which the evanescent wave of IR light is transmitted and incident onto the dye/TiO_2 layers before it is reflected internally multiple times and finally exits the sample and is detected by a fast recovery deuterated triglycine sulfate (DTGS) detector.

CONCLUSIONS

From a device perspective, it is no surprise that electrolyte/dye interactions will occur since their presence is mandated for a dye-regeneration process in the operational mechanism of a DSC. It is perhaps also not so surprising that dye regeneration will influence directly the dye-injection process, since the two processes form part of the same photovoltaic operational cycle.

However, the fact that these electrolyte/dye interactions have a substantial molecular effect on the nature of the dye/TiO_2 anchoring is a new finding. Indeed, it contrasts with many *ex situ* material characterization results, thereby underpinning the importance of developing *in situ* material characterization capabilities for DSC research. The contrast-matching strategy used in our *in situ* neutron reflectometry study has managed to witness these electrolyte/dye interactions experimentally by resolving a four-layer structural model to describe the electrolyte/dye/TiO_2 interface. The *in situ* nature of our structural results has also unraveled the molecular-level behavior of these interactions within a DSC device assembly. The close alignment of our results to molecular-dynamics simulations[45] is particularly encouraging. The consistency of our results with our supporting *ex situ* X-ray and neutron reflectometry, FTIR, and XPS experiments also compels us to conclude this discovery, although the *in situ* aspects of this work provide unique structural information within a DSC device. Indeed, this is a pioneering *in situ* structural determination of electrolyte/dye/TiO_2 interfaces within DSC device environments with contrast matching that nullified certain structural components to help (i) highlight certain structural features of interfacial layers and (ii) enable the co-refinement approach to fitting neutron reflectometry data, which afforded greater structural accuracy.

ASSOCIATED CONTENT

Supporting Information

Co-refinement of *ex situ* XR and NR data; determination of the relative extent of iodo species in the electrolyte layer atop the dye self-assembly; technical implementa- tion of the background subtraction for the *in situ* NR data; errors in background subtraction for the *in situ* neutron reflectometry data; *in situ* neutron reflectometry measurement, and sample alignment geometries; deter- mination of the thickness of the native SiO_2 layer on the silicon wafers; and dye/TiO_2 interfacial structures in the presence of acetonitrile and electrolyte components (PDF)

AUTHOR INFORMATION

Corresponding Author

Jacqueline M. Cole – *Cavendish Laboratory, Department of Physics, University of Cambridge, Cambridge CB3 0HE, United Kingdom; Research Complex at Harwell, Rutherford Appleton Laboratory, Didcot, Oxfordshire OX11 0FA, United Kingdom; ISIS Neutron and Muon Source, STFC Rutherford Appleton Laboratory, Didcot, Oxfordshire OX11 0QX, United Kingdom; Department of Chemical Engineering and Biotechnology, University of Cambridge, Cambridge CB3 0AS, United Kingdom; Argonne National Laboratory, Lemont, Illinois 60439, United States;* orcid.org/0000-0002-1552-8743; Email: jmc61@cam.ac.uk

Authors

Ke Deng – *Cavendish Laboratory, Department of Physics, University of Cambridge, Cambridge CB3 0HE, United Kingdom; Research Complex at Harwell, Rutherford Appleton Laboratory, Didcot, Oxfordshire OX11 0FA, United Kingdom*

Joshaniel F. K. Cooper – *ISIS Neutron and Muon Source, STFC Rutherford Appleton Laboratory, Didcot, Oxfordshire OX11 0QX, United Kingdom*

John R. P. Webster – *ISIS Neutron and Muon Source, STFC Rutherford Appleton Laboratory, Didcot, Oxfordshire OX11 0QX, United Kingdom*

Richard Haynes – *ISIS Neutron and Muon Source, STFC Rutherford Appleton Laboratory, Didcot, Oxfordshire OX11 0QX, United Kingdom*

Othman K. Al Bahri – *Cavendish Laboratory, Department of Physics, University of Cambridge, Cambridge CB3 0HE, United Kingdom; Research Complex at Harwell, Rutherford Appleton Laboratory, Didcot, Oxfordshire OX11 0FA, United Kingdom*

Nina-Juliane Steinke – *ISIS Neutron and Muon Source, STFC Rutherford Appleton Laboratory, Didcot, Oxfordshire OX11 0QX, United Kingdom*

Shaoliang Guan – *Research Complex at Harwell, Rutherford Appleton Laboratory, Didcot, Oxfordshire OX11 0FA, United Kingdom; Cardiff Catalysis Institute, School of Chemistry, Cardiff University, Cardiff CF10 3AT, United Kingdom;* orcid.org/0000-0002-0608-6584

Liliana Stan – *Argonne National Laboratory, Lemont, Illinois 60439, United States*

Xiaozhi Zhan – *Dongguan Neutron Science Center, Dongguan 523000, China*

Tao Zhu – *Beijing National Laboratory for Condensed Matter Physics and Institute of Physics, Chinese Academy of Sciences, Beijing 100190, China; Songshan Lake Materials Laboratory, Dongguan, Guangdong 523808, China*

Daniel W. Nye – *ISIS Neutron and Muon Source, STFC Rutherford Appleton Laboratory, Didcot, Oxfordshire OX11 0QX, United Kingdom*

Gavin B. G. Stenning – *ISIS Neutron and Muon Source, STFC Rutherford Appleton Laboratory, Didcot, Oxfordshire OX11 0QX, United Kingdom*

Author Contributions

J.M.C. conceived and designed the research project. J.M.C., K.D., R.H., J.F.K.C., and N.-J.S. designed and developed the bespoke sample environment needs for *in situ* neutron reflectometry on DSC device assemblies at the ISIS Neutron and Muon Source. L.S. and J.M.C. prepared the atomic-layer-deposited amorphous TiO_2 on silicon substrates; otherwise, K.D. prepared all of the samples for the project. K.D., J.F.K.C., J.M.C., and O.K.A. conducted the *in situ* neutron reflectometry experiments. K.D. undertook the neutron data analysis with assistance from J.F.K.C., J.M.C., and J.R.P.W. K.D. conducted the X-ray reflectometry experiments with support from G.B.G.S. and D.W.N. S.G. performed the X-ray photoelectron spectroscopy measurements, which were analyzed by K.D. K.D. carried out the infrared spectroscopy experiments and data analysis. K.D. performed *ex situ* neutron reflectometry experiments at the China Spallation Neutron Source, assisted by X.Z. and T.Z. K.D. and J.M.C. interpreted the results. J.M.C. led and coordinated the project and played the role of a Ph.D. supervisor to K.D. and O.K.A. J.R.P.W. gave neutron reflectometry senior expertise and local project oversight as ISIS management. J.M.C. wrote the manuscript. K.D. assisted

with the figures and drafted the SI. All authors provided input to the paper and proofread the final manuscript.

Funding

J.M.C. is indebted to the 1851 Royal Commission of the Great Exhibition for the 2014 Fellowship in Design, hosted by Argonne National Laboratory where work done was supported by the DOE Office of Science, Office of Basic Energy Sciences, and research resources from the Center for Nanoscale Materials, which is a DOE Office of Science Facility, all under contract no. DE-AC02-06CH11357. J.M.C. is also grateful for the BASF/Royal Academy of Engineering Research Chair in Data-Driven Molecular Engineering of Functional Materials, which is partly supported by the STFC *via* the ISIS Neutron and Muon Source. The STFC is also acknowledged for access to facilities at the ISIS Materials Characterisation Laboratory, STFC Rutherford Appleton Laboratory (RAL), and its funding provision for research carried out at the Research Complex at Harwell at RAL. XPS data collection was performed at the EPSRC National Facility for XPS ("HarwellXPS"), operated by Cardiff University and UCL, under Contract no. PR16195. O.K.A. acknowledges the Ministry of Higher Education (Oman) for sponsoring his Ph.D. research.

Notes

The authors declare no competing financial interest.

REFERENCES

(1) Gonçalves, L. M.; de Zea Bermudez, V.; Ribeiro, H. A.; Mendes, A. M. Dye-sensitized solar cells: A safe bet for the future. *Energy Environ. Sci.* 2008, *1*, 655−667.

(2) Pagliaro, M.; Palmisano, G.; Ciriminna, R.; Loddo, V. Nanochemistry aspects of titania in dye-sensitized solar cells. *Energy Environ. Sci.* 2009, *2*, 838−844.

(3) Xie, Z.; Jin, X.; Chen, G.; Xu, J.; Chen, D.; Shen, G. Integrated smart electrochromic windows for energy saving and storage applications. *Chem. Commun.* 2014, *50*, 608−610.

(4) Yoo, K.; Kim, J.-Y.; Lee, J. A.; Kim, J. S.; Lee, D.-K.; Kim, K.; Kim, J. Y.; Kim, B.; Kim, H.; Kim, W. M.; Kim, J. H.; Ko, M. J. Completely Transparent Conducting Oxide-Free and Flexible Dye-Sensitized Solar Cells Fabricated on Plastic Substrates. *ACS Nano* 2015, *9*, 3760−3771.

(5) Wen, Z.; Yeh, M.-H.; Guo, H.; Wang, J.; Zi, Y.; Xu, W.; Deng, J.; Zhu, L.; Wang, X.; Hu, C.; Zhu, L.; Sun, X.; Wang, Z. L. Self-powered textile for wearable electronics by hybridizing fiber-shaped nano-generators, solar cells, and supercapacitors. *Sci. Adv.* 2016, *2*, No. e1600097.

(6) Yun, M. J.; Cha, S. I.; Seo, S. H.; Kim, H. S.; Lee, D. Y. Insertion of Dye-Sensitized Solar Cells in Textiles using a Conventional Weaving Process. *Sci. Rep.* 2015, *5*, No. 11022.

(7) Peng, M.; Yu, X.; Cai, X.; Yang, Q.; Hu, H.; Yan, K.; Wang, H.; Dong, B.; Zhu, F.; Zou, D. Waveguide fiber dye-sensitized solar cells. *Nano Energy* 2014, *10*, 117−124.

(8) Liu, K.; Hsu, C.; Ni, J.; Ho, K.; Lin, K. Photovoltaic properties of dye-sensitized solar cells associated with amphiphilic structure of ruthenium complex dyes. *J. Colloid Interface Sci.* 2012, *372*, 73−79.

(9) Chen, H.; Cole, J. M.; Stenning, G. B. G.; Yanguas-Gil, A.; Elam, J. W.; Stan, L.; Gong, Y. Imaging Dye Aggregation in MK-2, N3, N749, and SQ-2 dye···TiO_2 Interfaces That Represent Dye-Sensitized Solar Cell Working Electrodes. *ACS Appl. Energy Mater.* 2020, *3*, 3230−3241.

(10) Cooper, C. B.; Beard, E. J.; Vazquez-Mayagoitia, Á.; Stan, L.; Stenning, G. B. G.; Nye, D. W.; Vigil, J. A.; Tomar, T.; Jia, J.; Bodedla, G. B.; Chen, S.; Gallego, L.; Franco, S.; Carella, A.; Thomas, K. R. J.; Xue, S.; Zhu, X.; Cole, J. M. Design-to-Device Approach Affords Panchromatic Co-Sensitized Solar Cells. *Adv. Energy Mater.* 2019, *9*, No. 1802820.

(11) Voïtchovsky, K.; Ashari-Astani, N.; Tavernelli, I.; Tétreault, N.; Rothlisberger, U.; Stellacci, F.; Grätzel, M.; Harms, H. A. In Situ Mapping of the Molecular Arrangement of Amphiphilic Dye Molecules at the TiO_2 Surface of Dye-Sensitized Solar Cells. *ACS Appl. Mater. Interfaces* 2015, *7*, 10834−10842.

(12) Ikeda, M.; Koide, N.; Han, L.; Sasahara, A.; Onishi, H. Scanning Tunneling Microscopy Study of Black Dye and Deoxycholic Acid Adsorbed on a Rutile TiO_2(110). *Langmuir* 2008, *24*, 8056−8060.

(13) Kley, C. S.; Dette, C.; Rinke, G.; Patrick, C. E.; Čechal, J.; Jung, S. J.; Baur, M.; Dürr, M.; Rauschenbach, S.; Giustino, F.; Stepanow, S.; Kern, K. Atomic-Scale Observation of Multiconformational Binding and Energy Level Alignment of Ruthenium-Based Photosensitizers on TiO_2 Anatase. *Nano Lett.* 2014, *14*, 563−569.

(14) Deng, K.; Cole, J. M.; Rawle, J. L.; Nicklin, C.; Chen, H.; Yanguas-Gil, A.; Elam, J. W.; Stenning, G. B. G. Dye Nanoaggregate Structures in MK-2, N3, and N749 Dye···TiO_2 Interfaces That Represent Dye-Sensitized Solar Cell Working Electrodes. *ACS Appl. Energy Mater.* 2020, *3*, 900−914.

(15) Griffith, M. J.; James, M.; Triani, G.; Wagner, P.; Wallace, G. G.; Officer, D. L. Determining the Orientation and Molecular Packing of Organic Dyes on a TiO_2 Surface Using X-ray Reflectometry. *Langmuir* 2011, *27*, 12944−12950.

(16) McCree-Grey, J.; Cole, J. M.; Evans, P. J. Preferred Molecular Orientation of Coumarin 343 on TiO_2 Surfaces: Application to Dye-Sensitized Solar Cells. *ACS Appl. Mater. Interfaces* 2015, *7*, 16404−16409.

(17) McCree-Grey, J.; Cole, J. M.; Holt, S. A.; Evans, P. J.; Gong, Y. Dye···TiO_2 interfacial structure of dye-sensitised solar cell working electrodes buried under a solution of I^-/I_3^- redox electrolyte. *Nanoscale* 2017, *9*, 11793−11805.

(18) Cole, J. M.; Gong, Y.; McCree-Grey, J.; Evans, P. J.; Holt, S. A. Modulation of N3 and N719 dye···TiO_2 Interfacial Structures in Dye-Sensitized Solar Cells As Influenced by Dye Counter Ions, Dye Deprotonation Levels, and Sensitizing Solvent. *ACS Appl. Energy Mater.* 2018, *1*, 2821−2831.

(19) Shklover, V.; Nazeeruddin, M.-K.; Zakeeruddin, S. M.; Barbé, C.; Kay, A.; Haibach, T.; Steurer, W.; Hermann, R.; Nissen, H.-U.; Grätzel, M. Structure of Nanocrystalline TiO_2 Powders and Precursor to Their Highly Efficient Photosensitizer. *Chem. Mater.* 1997, *9*, 430−439.

(20) Cole, J. M.; Low, K. S.; Gong, Y. Discovery of Black Dye Crystal Structure Polymorphs: Implications for Dye Conformational Variation in Dye-Sensitized Solar Cells. *ACS Appl. Mater. Interfaces* 2015, *7*, 27646−27653.

(21) Low, K. S.; Cole, J. M.; Zhou, X.; Yufa, N. S. Rationalizing the molecular origins of Ru- and Fe-based dyes for dye-sensitized solar cells. *Acta Crystallogr., Sect. B: Struct. Sci.* 2012, *68*, 137−149.

(22) Cole, J. M.; Low, K. S.; Ozoe, H.; Stathi, P.; Kitamura, C.; Kurata, H.; Rudolf, P.; Kawase, T. Data mining with molecular design rules identifies new class of dyes for dye-sensitised solar cells. *Phys. Chem. Chem. Phys.* 2014, *16*, 26684−26690.

(23) Cole, J. M.; Blood-Forsythe, M. A.; Lin, T. C.; Pattison, P.; Waddell, P. G.; Zhang, L.; Koumura, N.; Mori, S. Discovery of S··· C□N Intramolecular Bonding in a Thiophenylcyanoacrylate-Based Dye: Realizing Charge Transfer Pathways and Dye···TiO_2 Anchoring Characteristics for Dye-Sensitized Solar Cells. *ACS Appl. Mater. Interfaces* 2017, *9*, 25952−25961.

(24) Mukaddem, K. T.; Chater, P. A.; Devereux, L. R.; Al Bahri, O. K.; Jain, A.; Cole, J. M. Dye-Anchoring Modes at the Dye···TiO_2 Interface of N3- and N749-Sensitized Solar Cells Revealed by Glancing-Angle Pair Distribution Function Analysis. *J. Phys. Chem. C* 2020, *124*, 11935−11945.

(25) Pazoki, M.; Cappel, U. B.; Johannson, E. M. J.; Hagfeldt, A.; Boschloo, G. Characterization techniques for dye-sensitized solar cells. *Energy Environ. Sci.* 2017, *10*, 672−709.

(26) Feldt, S. M.; Cappel, U. B.; Johansson, E. M. J.; Boschloo, G.; Hagfeldt, A. Characterization of Surface Passivation by Poly-

(methylsiloxane) for Dye-Sensitized Solar Cells Employing the Ferrocene Redox Couple. *J. Phys. Chem. C* 2010, *114*, 10551−10558.
(27) Alarcon H.; Hedlund, M.; Johansson, E. M. J.; Rensmo, H.; Hagfeldt, A.; Boschloo, G. Modification of Nanostructured TiO_2 Electrodes by Electrochemical Al^{3+} Insertion: Effects on Dye-Sensitized Solar Cell Performance. *J. Phys. Chem. C* 2007, *111*, 13267−13274.
(28) Schiffmann, F.; VandeVondele, J.; Hutter, J.; Wirz, R.; Urakawa, A.; Baiker, A. Protonation-Dependent Binding of Ruthenium Bipyridyl Complexes to the Anatase(101) Surface. *J. Phys. Chem. C* 2010, *114*, 8398−8404.
(29) Yu, S.; Ahmadi, S.; Zuleta, M.; Tian, H.; Schulte, K.; Pietzsch, A.; Hennies, F.; Weissenrieder, J.; Yang, X.; Göthelid, M. Adsorption geometry, molecular interaction, and charge transfer of triphenyl-amine-based dye on rutile TiO_2(110). *J. Chem. Phys.* 2010, *133*, No. 224704.
(30) Brennan, T. P.; Tanskanen, J. T.; Bakke, J. R.; Nguyen, W. H.; Nordlund, D.; Toney, M. F.; McGehee, M. D.; Sellinger, A.; Bent, S. F. Dynamical Orientation of Large Molecules on Oxide Surfaces and its Implications for Dye-Sensitized Solar Cells. *Chem. Mater.* 2013, *25*, 4354−4363.
(31) Gutierrez-Sosa, A.; Martínez-Escolano, P.; Raza, H.; Lindsay, R.; Wincott, P. L.; Thornton, G. Orientation of carboxylates on TiO_2(1 1 0). *Surf. Sci.* 2001, *471*, 163−169.
(32) Rienzo, A.; Mayor, L. C.; Magnano, G.; Satterley, C. J.; Ataman, E.; Schnadt, J.; Schulte, K.; O'Shea, J. N. X-ray absorption and photoemission spectroscopy of zinc protoporphyrin adsorbed on rutile TiO_2(110) prepared by in situ electrospray deposition. *J. Chem. Phys.* 2010, *132*, No. 084703.
(33) Westermark, K.; Rensmo, H.; Siegbahn, H.; Keis, K.; Hagfeldt, A.; Ojamae, L.; Persson, P. PES Studies of $Ru(dcbpyH_2)_2(NCS)_2$ Adsorption on Nanostructured ZnO for Solar Cell Applications. *J. Phys. Chem. B* 2002, *106*, 10102−10107.
(34) McCree-Grey, J. Molecular Orientation Dynamics of Dyes in Dye-Sensitized Solar Cells. Ph.D. Dissertation, University of Cambridge, 2016.
(35) Nazeeruddin, M. K.; Kay, A.; Rodicio, I.; Humphry-Baker, R.; Mueller, E.; Liska, P.; Vlachopoulos, N.; Graetzel, M. Conversion of light to electricity by *cis*-X_2bis(2,2′-bipyridyl-4,4′-dicarboxylate)-ruthenium(II) charge-transfer sensitizers (X = Cl^-, Br^-, I^-, CN^-, and SCN^-) on nanocrystalline titanium dioxide electrodes. *J. Am. Chem. Soc.* 1993, *115*, 6382−6390.
(36) Nazeeruddin, M. K.; Pechy, P.; Graetzel, M. Efficient panchromatic sensitization of nanocrystalline TiO_2 films by a black dye based on a trithiocyanato−ruthenium complex. *Chem. Commun.* 1997, 1705−1706.
(37) Koumura, N.; Wang, Z.-S.; Mori, S.; Miyashita, M.; Suzuki, E.; Hara, K. Alkyl-Functionalized Organic Dyes for Efficient Molecular Photovoltaics. *J. Am. Chem. Soc.* 2006, *128*, 14256−14257.
(38) Koumura, N.; Wang, Z.-S.; Mori, S.; Miyashita, M.; Suzuki, E.; Hara, K. Addition/Correction to Alkyl-Functionalized Organic Dyes for Efficient Molecular Photovoltaics [*J. Am. Chem. Soc.* 2006, 128, 14256-14257]. *J. Am. Chem. Soc.* 2008, *130*, 4202−4203.
(39) Hagfeldt, A.; Boschloo, G.; Sun, L.; Kloo, L.; Pettersson, H. Dye-Sensitized Solar Cells. *Chem. Rev.* 2010, *110*, 6595−6663.
(40) Zhang, L.; Cole, J. M. Anchoring Groups for Dye-Sensitized Solar Cells. *ACS Appl. Mater. Interfaces* 2015, *7*, 3427−3455.
(41) Sasahara, A.; Pang, C. L.; Onishi, H. STM Observation of a Ruthenium Dye Adsorbed on a TiO_2(110) Surface. *J. Phys. Chem. B* 2006, *110*, 4751−4755.
(42) Sears, V. F. Neutron scattering lengths and cross sections. *Neutron News* 1992, *3*, 26−37.
(43) Tateyama, Y.; Sumita, M.; Ootani, Y.; Aikawa, K.; Jono, R.; Han, L.; Sodeyama, K. Acetonitrile Solution Effect on Ru N749 Dye Adsorption and Excitation at TiO_2 Anatase Interface. *J. Phys. Chem. C* 2014, *118*, 16863−16871.
(44) Privalov, T.; Boschloo, G.; Hagfeldt, A.; Svensson, P. H.; Kloo, L. A Study of the Interactions between I^-/I_3^- Redox Mediators and Organometallic Sensitizing Dyes in Solar Cells. *J. Phys. Chem. C* 2009, *113*, 783−790.
(45) Schiffmann, F.; VandeVondele, J.; Hutter, J.; Urakawa, A.; Wirz, R.; Baiker, A. An atomistic picture of the regeneration process in dye sensitized solar cells. *Proc. Natl. Acad. Sci. U.S.A.* 2010, *107*, 4830−4833.
(46) Labat, F.; Ciofinia, I.; Adamo, C. Revisiting the importance of dye binding mode in dye-sensitized solar cells: a periodic viewpoint. *J. Mater. Chem.* 2012, *22*, 12205−12211.
(47) Clark, R. J. H.; Williams, C. S. Infra-red spectra (3000-200 cm^{-1}) of metal-isothiocyanate complexes. *Spectrochim. Acta* 1966, *22*, 1081−1090.
(48) Kitson, R. E.; Griffith, N. E. Infrared Absorption Band Due to Nitrile Stretching Vibration. *Anal. Chem.* 1952, *24*, 334−337.
(49) *NIST X-ray Photoelectron Spectroscopy Database*, NIST Standard Reference Database Number 20; National Institute of Standards and Technology: Gaithersburg, MD, 2000 (last accessed April 17, 2020).
(50) For XPS Ti 2p data of N_3 on TiO_2 (general), see: Patrochínio, A. O. T.; Paniago, E. B.; Paniago, R. M.; Murakami Iha, N. Y. XPS characterization of sensitized n-TiO_2 thin films for dye-sensitized solar cell applications. *Appl. Surf. Sci.* 2008, *254*, 1874−1879.
(51) For XPS Ti 2p data of N3 on TiO_2, see Figure S10 in: Wayment-Steele, H. K.; Johnson, L. E.; Tian, F.; Dixon, M. C.; Benz, L.; Johal, M. S. Monitoring N3 Dye Adsorption and Desorption on TiO_2 Surfaces: A Combined QCM-D and XPS Study *ACS Appl. Mater. Interfaces*. 2014, *6*, 9093 9099 DOI: 10.1021/am500920w.
(52) Clifford, J. N.; Palomares, E.; Md. Nazeeruddin, K.; Grätzel, M.; Durrant, J. R. Dye Dependent Regeneration Dynamics in Dye Sensitized Nanocrystalline Solar Cells: Evidence for the Formation of a Ruthenium Bipyridyl Cation/Iodide Intermediate. *J. Phys. Chem. C* 2007, *111*, 6561−6567.
(53) Li, X.; Reynal, A.; Barnes, P.; Humphry-Baker, R.; Zakeeruddin, S. M.; De Angelis, F.; O'Regan, B. C. Measured Binding Coefficients for Iodine and Ruthenium Dyes; Implications for Recombination in Dye Sensitised Solar Cells. *Phys. Chem. Chem. Phys.* 2012, *14*, 15421−15428.
(54) Simon, S. J. C.; Parlane, F. G. L.; Swords, W. B.; Kellett, C. W.; Du, C.; Lam, B.; Dean, R. K.; Hu, K.; Meyer, G. J.; Berlinguette, C. P. Halogen Bonding Promotes Higher Dye-Sensitized Solar Cell Photovoltages. *J. Am. Chem. Soc.* 2016, *138*, 10406−10409.
(55) Webster, J.; Holt, S.; Dalgliesh, R. INTER the chemical interfaces reflectometer on target station 2 at ISIS. *Phys. B* 2006, *385−386*, 1164−1166.
(56) Arnold, O.; Bilheux, J. C.; Borreguero, J. M.; Buts, A.; Campbell, S. I.; Chapon, L.; Doucet, M.; Draper, N.; Ferraz Leal, R.; Gigg, M. A.; Lynch, V. E.; Markvardsen, A.; Mikkelson, D. J.; Mikkelson, R. L.; Miller, R.; Palmen, K.; Parker, P.; Passos, G.; Perring, T. G.; Peterson, P. F.; Ren, S.; Reuter, M. A.; Savici, A. T.; Taylor, J. W.; Taylor, R. J.; Tolchenov, R.; Zhou, W.; Zikovsky, J. Mantid□Data analysis and visualization package for neutron scattering and μSR experiments. *Nucl. Instrum. Methods Phys. Res., Sect. A* 2014, *764*, 156−166.
(57) Björck, M.; Andersson, G. GenX: an extensible X-ray reflectivity refinement program utilizing differential evolution. *J. Appl. Crystallogr.* 2007, *40*, 1174−1178.
(58) Zhu, T.; Zhan, X.; Xiao, S.; Sun, Y.; Wu, Y.; Zhou, A.; Han, Q. MR: The multipurpose reflectometer at CSNS. *Neutron News* 2018, *29*, 11−13.
(59) Li, Q.; Wang, L.-M.; Liu, S.; Zhan, X.; Zhu, T.; Cao, Z.; Lai, H.; Zhao, J.; Cai, Y.; Xie, W.; Huang, F. Impact of Donor−Acceptor Interaction and Solvent Additive on the Vertical Composition Distribution of Bulk Heterojunction Polymer Solar Cells. *ACS Appl. Mater. Interfaces* 2019, *11*, 45979−45990.
(60) Wang, L.-M.; Li, Q.; Liu, S.; Cao, Z.; Cai, Y.-P.; Jiao, X.; Lai, H.; Xie, W.; Zhan, X.; Zhu, T. Quantitative Determination of the Vertical Segregation and Molecular Ordering of PBDB-T/ITIC Blend Films with Solvent Additives. *ACS Appl. Mater. Interfaces* 2020, *12*, 24165−24173.